JPEDAV (2005) 26:487-493
DOI: 10.1361/154770305X66592
1547-7037/$19.00 ©ASM International

Internal Corrosion of Engineering Alloys: Experiment and Computer Simulation

Ulrich Krupp and Hans J. Christ

(Submitted July 18, 2005)

High-temperature corrosion is generally known as a material degradation process that occurs at the surface of engineering components. In the case of internal corrosion, the corrosive species penetrates into the material by solid-state diffusion leading to the formation of internal precipitates, for instance, oxides (internal oxidation), nitrides (internal nitridation), and carbides (carburization). It is known from numerous publications and technical failure cases that internal corrosion results in a strong deterioration of the properties of a material (i.e., near-surface embrittlement or the dissolution of strengthening phases). The present article introduces the classic theory of internal oxidation and reviews some recent research on internal corrosion phenomena that are closely related to the failure mechanisms of thermally grown protective oxide scales on several commercial high-temperature alloys (e.g., single-crystalline and polycrystalline Ni-base alloys and Cr steels). The mechanisms and kinetics of internal corrosion processes are determined by the temperature, the local chemical composition of the material, the solubility and diffusivity of the corrosive species, as well as the mechanical loading conditions. These influence factors are taken into account by means of a computer model combining a numerical finite-difference approach to solve the diffusion differential equations with the thermodynamic tool ChemApp. Using several examples, it is shown that the model has been applied successfully to simulate the internal nitridation, carburization, and oxidation of high-temperature alloys.

1. Introduction

Internal corrosion is a generic kind of material degradation occurring at high temperatures that is driven by the inward diffusion of a corrosive species (i.e., oxygen, nitrogen, carbon, or sulfur, followed by internal precipitation of the respective oxides, nitrides, carbides, and sulfides).[1] Contrary to the formation of superficial scales, which in the case of Cr_2O_3 and Al_2O_3 protect the substrate against excessive corrosion attack,[2] internal corrosion may result in a deep deterioration of the physical properties of the material (e.g., creep resistance and high-temperature fatigue strength).[3,4] Figure 1 shows an example of internal oxidation (Al_2O_3) and nitridation (AlN; penetration depth ξ = 600 μm) underneath a thin Cr_2O_3 scale.

The mechanism of internal corrosion depends on the local concentrations and the diffusivities of the corrosive species and the metallic elements in the substrate. For the example shown in Fig. 1, a low oxygen partial pressure, $p(O_2)$, relative to the nitrogen partial pressure $p(N_2)$ in the combustion gas leads to conditions in the material interior, for which AlN instead of Al_2O_3 is the thermodynamically most stable compound.*

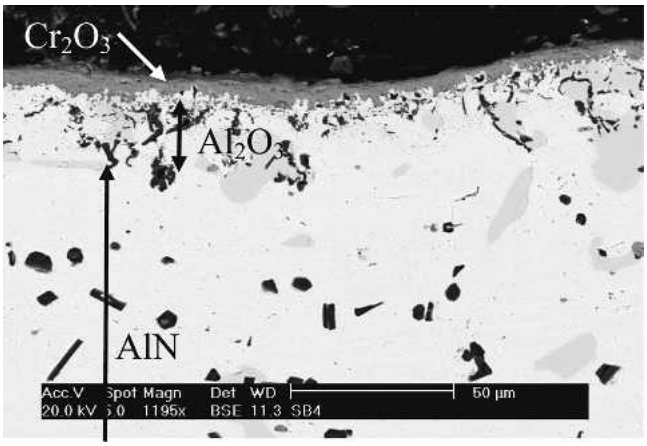

Fig. 1 Internal oxidation and nitridation attack of a failed natural gas burner tube of alloy 601 operated at T = 1100 °C

Even in the case of Al_2O_3-scale-forming Ni-base superalloys designed for the use at very high temperatures and mechanical load, repeated failure of the protective oxide scale by spalling and cracking can result in a transition from external to internal oxidation and hence, in the occurrence of breakaway oxidation in combination with massive internal corrosion (Al_2O_3, Cr_2O_3, AlN, and TiN). Due to the high specific volume of the internal corrosion products compared with that of the alloy, mechanical stresses arise that may lead to crack formation (Fig. 2).[5]

This article is a revised version of the paper printed in the *Proceedings of the First International Conference on Diffusion in Solids and Liquids—DSL-2005*, Aveiro, Portugal, July 6-8, 2005, Andreas Öchsner, José Grácio and Frédéric Barlat, eds., University of Aveiro, 2005.

Ulrich Krupp and **Hans J. Christ,** Universität Siegen, Institut für Werkstofftechnik Paul-Bonatz Str. 9-11, 57068 Siegen, Germany. Contact e-mail: ulrich.krupp@uni-siegen.de.

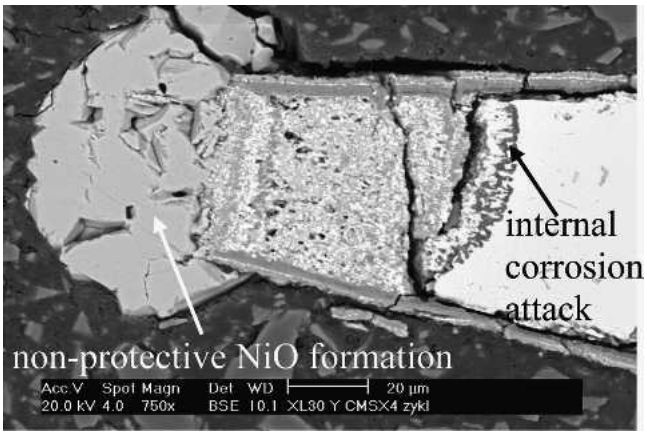

Fig. 2 Internal oxidation and nitridation as a consequence of oxide-scale failure in a wedge-type specimen of the single-crystalline Ni-base superalloy CMSX-4 at $T = 1100$ °C[5]

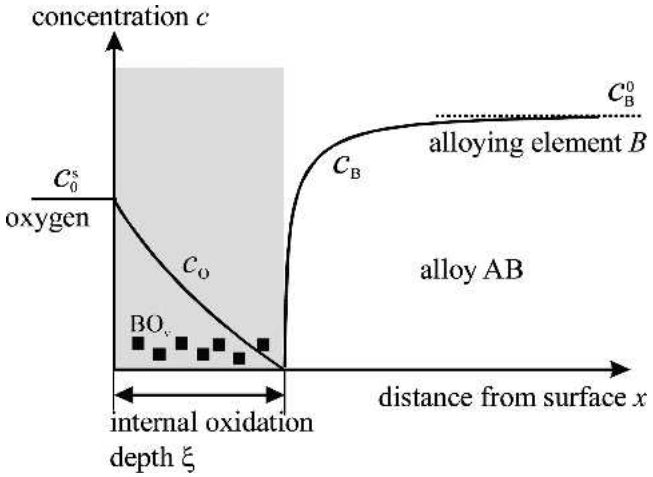

Fig. 3 Concentration profiles during internal precipitation of BO_v according to the classic theory of internal oxidation

2. The Classic Theory of Internal Oxidation

A very fundamental and frequently used treatment of internal oxidation representing many internal corrosion problems was published by Wagner[6] in 1959 in an article discussing some special features of the oxidation of alloys compared with the oxidation of pure substances and has been termed the *classical theory of internal oxidation*.

Assuming that internal oxidation of BO_v in an alloy *AB* is governed by diffusion processes as described by the differential equation for the time-dependent and location-dependent concentration *c*:

$$\frac{\partial c}{\partial t} = \nabla(D\nabla c) \qquad \text{(Eq 1)}$$

or simplified for only one dimension *x*, and concentration-independent diffusion coefficients for oxygen and the oxide-forming metallic solute B $D_{O/B}$:

$$\frac{\partial c_{O/B}}{\partial t} = D_{O/B}\frac{\partial^2 c_{O/B}}{\partial x^2} \qquad \text{(Eq 2)}$$

the depth of the internal-oxidation reaction front ξ can be given by a parabolic relationship:

$$\xi(t) = 2\gamma\sqrt{D_O t} \qquad \text{(Eq 3)}$$

where γ is a parameter to be determined. The differential Eq 2 can be solved by taking boundary conditions into account (Fig. 3): (1) the oxygen concentration c_O at the surface ($x = 0$) is constant ($c_O = c_O^s$), while (2) ahead of the internal-oxidation depth $x \geq \xi$ it is zero; (3) the solute concentration c_B is 0 within the internal-oxidation depth $x \leq \xi$; (4) at the beginning ($t = 0$), c_B is everywhere ($x \geq 0$) equal to the initial solute concentration c_B^0. Hence, according to Fig. 3, the oxygen concentration c_O and the metal concentration c_B can be written as follows:

$$c_O = c_O^S\left[1 - \frac{\mathrm{erf}(x/2\sqrt{D_O t})}{\mathrm{erf}\,\gamma}\right] \qquad \text{(Eq 4)}$$

$$c_B = c_B^0\left[1 - \frac{\mathrm{erfc}(x/2\sqrt{D_B t})}{\mathrm{erfc}\,(\gamma\sqrt{D_O/D_B})}\right] \qquad \text{(Eq 5)}$$

Because at the reaction front ($x = \xi$) the oxygen flux must be equivalent to the metal flux:

$$\lim_{\varepsilon\to 0}\left[-D_O\left(\frac{\partial c_O}{\partial x}\right)_{x=\xi-\varepsilon} = \nu D_B\left(\frac{\partial c_B}{\partial x}\right)_{x=\xi+\varepsilon}\right] \qquad \text{(Eq 6)}$$

the problem can be solved, and Eq 3 to 6 yield, together with a few simplifying assumptions (see Ref 6 for details), the governing equation for internal oxidation, where k_0 is the internal oxidation constant:

$$\xi^2 = 2k_0 t \cong 2\frac{D_O c_O^s}{\nu c_B^0}t \qquad \text{(Eq 7)}$$

under the condition $D_B/D_0 << c_0^s/c_B^0 << 1$. If the solute diffusivity D_B is not negligible with respect to the oxygen diffusivity D_O (i.e., $c_O^s/c_B^0 << D_B/D_O << 1$), the following expression for the internal-oxidation penetration depth ξ is valid:

$$\xi^2 = \frac{\pi D_O^2 {c_O^s}^2}{\nu^2 {c_B^0}^2 D_B}t \qquad \text{(Eq 8)}$$

Then, the solute B might become enriched within the internal-oxidation zone, and the oxides tend to grow together. Transition from internal to external oxidation can be expected when the initial B concentration in the alloy exceeds a value given by Eq 9, which depends on a critical volume fraction of oxide g^*, having in the case of internal oxidation of Ag-In alloys[7] a value of $g^* = 0.3$.

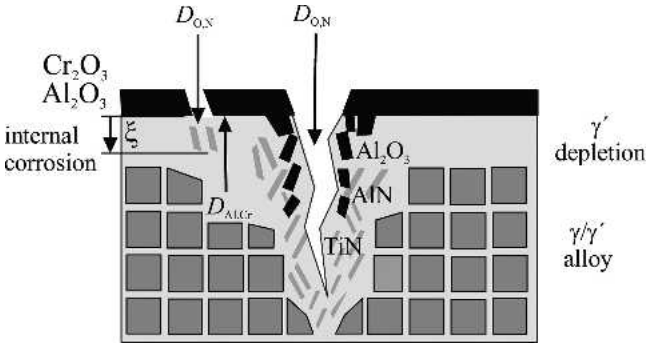

Fig. 4 Schematic representation of complex internal corrosion processes as a consequence of oxide scale failure

$$c_B^0 < \frac{\pi g^* D_O V}{2\nu D_B V_{BO_\nu}} c_O^s \quad \text{(Eq 9)}$$

Despite the perspicuity and the versatility of Wagner's theory, there are several limitations that restrict its application to the solution of simple internal-corrosion problems and allows merely an estimative treatment of more complex cases. Consequently, the theory of internal oxidation was permanently extended and critically discussed[8] (e.g., with respect to the simultaneous occurrence of superficial oxide scale formation and internal precipitation of one[9] or more compounds of high or low stability and various morphologies[10]). In the latter case, the assumption of the solubility product being 0 is an oversimplification (i.e., the local thermodynamic equilibrium needs to be taken into account). Furthermore, diffusion through the internal oxidation zone cannot necessarily be set equal to bulk diffusion through the substrate lattice. As proposed by Stott et al.,[11] the diffusion flux depends substantially on interfacial transport mechanisms, which of course may vary with the substrate microstructure or the morphology and density of the precipitates themselves.[12] The internal-corrosion situation as a consequence of oxide scale failure schematically represented in Fig. 4 summarizes the physical phenomena that have to be taken into account within mechanism-based modeling concepts.

3. Numerical Modeling of Internal Corrosion Processes

The combination of multicomponent bulk and grain-boundary diffusion with computational thermochemistry requires a numerical solution of the diffusion differential equation (Eq 1) in the following equation, which has been simplified for two-dimensional problems:

$$\frac{\partial c}{\partial t} = D_x \frac{\partial^2 c}{\partial x^2} + D_y \frac{\partial^2 c}{\partial y^2} \quad \text{(Eq 10)}$$

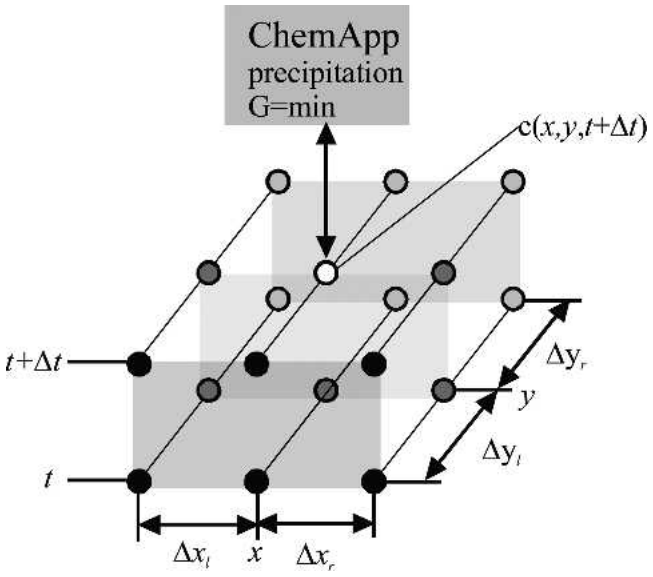

Fig. 5 Schematic representation of the two-dimensional finite-difference mesh (Crank-Nicolson scheme) applied in combination with ChemApp

According to the Crank-Nicolson scheme of the finite-difference method,[13] Eq 10 can be expressed by replacing the derivatives by difference quotients using time steps of length Δt and location steps of flexible widths Δx and Δy, respectively (l = left-hand side; r = right-hand side, according to Fig. 5):

$$\begin{aligned}
&\frac{c(x, y, t+\Delta t) - c(x, y, t)}{\Delta t} \\
&= \frac{D_x(x, y)}{2}\left(\frac{c(x-\Delta x, y, t) - 2c(x, y, t) + c(x+\Delta x, y, t)}{\Delta x_l(x, y)\cdot \Delta x_r(x, y)}\right. \\
&\left. + \frac{c(x-\Delta x, y, t+\Delta t) - 2c(x, y, t+\Delta t) + c(x+\Delta x, y, t+\Delta t)}{\Delta x_l(x, y)\cdot \Delta x_r(x, y)}\right) \\
&+ \frac{D_y(x, y)}{2}\left(\frac{c(x, y-\Delta y, t) - 2c(x, y, t) + c(x, y+\Delta y, t)}{\Delta y_l(x, y)\cdot \Delta y_r(x, y)}\right. \\
&\left. + \frac{c(x, y-\Delta y, t+\Delta t) - 2c(x, y, t+\Delta t) + c(x, y+\Delta y, t+\Delta t)}{\Delta y_l(x, y)\cdot \Delta y_r(x, y)}\right)
\end{aligned} \quad \text{(Eq 11)}$$

Equation 11 allows the stepwise solution of diffusion problems in a two-dimensional area of the size $n \times \Delta x \times m \times \Delta x$ using location-dependent diffusion coefficients $D_x(x,y)$ (x direction) and $D_y(x,y)$ (y direction), respectively, to accommodate for bulk and interfacial diffusion at the same time.

The set of concentrations $c(x,y,t + \Delta t)$ for all of the species participating in the corrosion process is obtained by an array of concentrations at the preceding time step according to Fig. 5 and Eq 11. Prior to the continuation of the calculation for the time step $t + 2\Delta t$, the concentrations at t

+ Δt are corrected according to local thermodynamic equilibrium at x,y by means of ChemApp (GTT Technologies, Herzogenrath, Germany) subroutines. ChemApp is a commercial thermodynamic software package that is based on the concept of Gibbs energy (G) minimization for multiphase systems according to:

$$G = \sum_{j=1}^{m} c_j \, (G_{j,pure} + G_{j,id} + G_{j,non-id}) = \min \qquad \text{(Eq 12)}$$

where for the sum of the phases j present in the system the minimum of G is determined in an iterative way for an initially unknown chemical composition of the system.[14] The contributions of the pure substances $G_{j,pure}$, the ideal mixing $G_{j,id}$, and the excess energy of nonideal mixing $G_{j,non-id}$ are calculated by means of tailor-made thermochemical databases.

The computer model, which was originally developed for internal carburization[15] and internal nitridation,[16] has been implemented in a parallel-computing MatLab (The MathWorks, Inc., Natick, MA) environment enabling the treatment of complex corrosion processes that are governed by interfacial and bulk diffusion in combination with chemical reactions of the diffusing species.

The next section gives examples of how internal-corrosion problems can be treated by both experimental methods and computer simulations.

4. Internal Nitridation of Ni-Base Alloys

The most common way to study high-temperature corrosion is a combination of thermogravimetric kinetics measurements (i.e., weight change versus time) and microstructural analysis of corrosion products [e.g., by analytical scanning electron microscopy (SEM), transmission electron microscopy, or x-ray diffraction].

Figure 5(a) shows SEM micrographs of cross sections through the near-surface layer of two Ni-Cr-Ti alloys that were exposed to a nitrogen-based atmosphere at 1100 °C (50 vol.% N_2, 45 vol.% He, 5 vol.% H_2 + Ti sponge as an oxygen getter $=> p(N_2) = 0.5$bar, $p(O_2) \approx 10^{-18}$bar).[17] Even though the concentration of the internal nitride-forming element Ti was constant, the internal precipitation depth of TiN in the Ni-20wt.%Cr-2wt.%Ti alloy is substantially higher than that in the Ni-5wt.%Cr-2wt.%Ti alloy. Similar results were obtained for the Ni-$x$wt.%Cr-2wt.%Ti-2wt.%Al alloys studied. Cr-nitride formation was not observed for alloys having an initial Cr concentration of $c_{Cr} \leq$ 20 wt.%. Only in the case of Ni-30wt.%Cr-2wt.%Ti the formation of internal Cr_2N and the ternary π phase ($Cr_{12.8}Ni_{7.2}N_4$), in addition to internal TiN precipitation, was observed.[18]

A summarizing evaluation of internal nitridation kinetics for TiN precipitation in Ni-$x$wt.%Cr-2wt.%Ti is shown in Fig. 6(b), where the experimentally measured TiN penetration depths are represented as nitridation constants k_N according to the parabolic rate law in Eq 7 versus the initial Cr concentration.

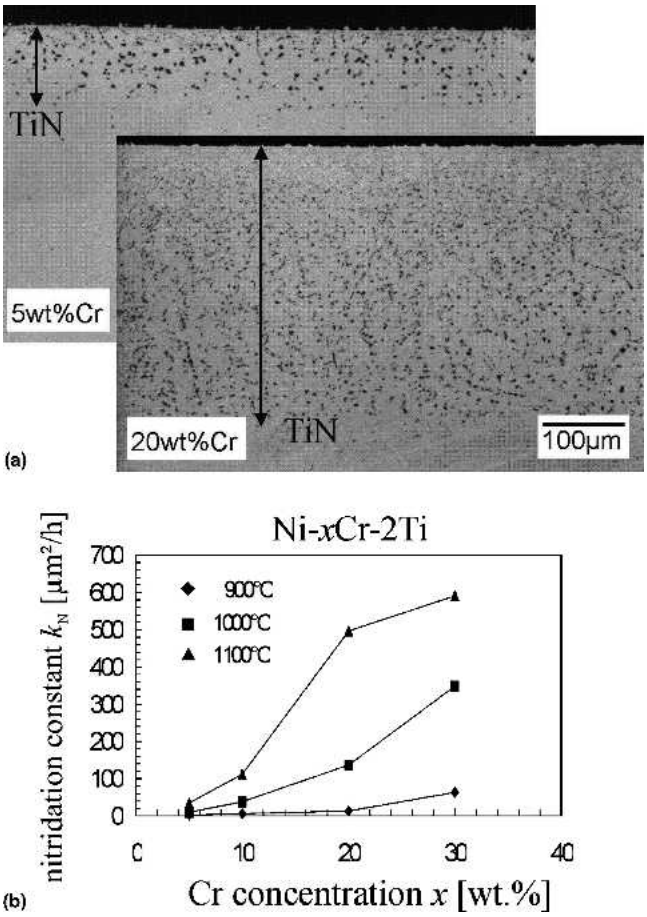

Fig. 6 (a) Internal nitridation of Ni-5wt.%Cr-2wt.%Ti and Ni-20wt.%Cr-2wt.%Ti alloys (100 h, 1100 °C, N_2) and (b) corresponding nitridation constants k_N (according to the internal oxidation constant in Eq 7)[17]

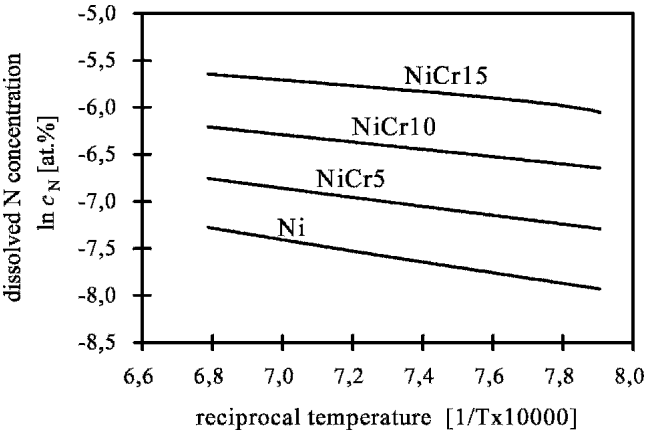

Fig. 7 Arrhenius-type plot of the maximum dissolved N concentration in various Ni-Cr alloys versus the reciprocal temperature[19]

The strong effect of the Cr content on the internal nitridation behavior of Ni-base alloys was attributed to an increase in the maximum nitrogen solubility. This is shown by the Arrhenius plot in Fig. 7 representing results obtained

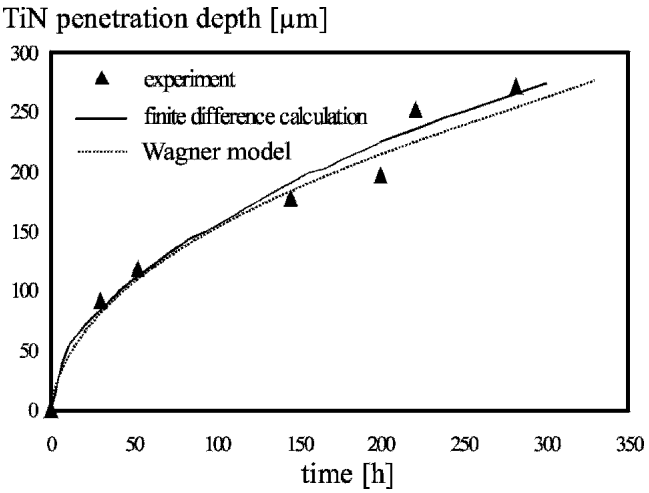

Fig. 8 Experimentally determined and calculated TiN penetration depth in Ni-20wt.%Cr-2wt.%Ti alloy (100 h, 1100 °C, nitrogen-based atmosphere)

by thermodynamic calculations using the commercial software ChemSage/FactSage (GTT Technologies, Herzogenrath, Germany) in combination with a database for the system Ni-Cr-Al-Ti-N. The various lines correspond to different concentrations of Cr in Ni. The concentrations of Al and Ti within the zone of internal nitridation are negligible as a consequence of the rather high stability of the TiN and AlN formed, so that the effect of these elements on the nitrogen solubility can be neglected.

By setting the surface concentration of the solute c_0^s in Eq 7 equal to the maximum N concentration soluble in Ni-base alloys, as calculated by ChemSage/FactSage, the diffusion coefficient was estimated by:

$$D_N \cong \frac{k_N c_B^0}{c_O^s} \cong \frac{\xi^2 c_B^0}{2tc_O^s} \quad \text{(Eq 13)}$$

yielding, for example, an effective diffusion coefficient D_N for N within a TiN precipitation zone in Ni-20wt.%Cr[17] of:

$$D_N \cong 4.7 \cdot 10^{-6} \frac{m^2}{s} \exp \frac{-125.72 kJ/mol}{RT} \quad \text{(Eq 14)}$$

The estimated diffusion coefficients together with the thermochemical database served as input data for the finite-difference computer simulation of internal nitridation of Ni-base alloys. Figure 8 demonstrates the excellent agreement between experimentally measured TiN precipitation depths and the simulated internal nitridation kinetics. It is worth mentioning that, in the case of the internal precipitation of TiN as a very stable compound, the restrictions for the applicability of the classic theory of internal oxidation are fulfilled (i.e., the experimental data points in Fig. 8 can be fitted by the parabolic rate law in Eq 7).

The exposure of quaternary alloys of the system Ni-Cr-Al-Ti to the nitrogen-based atmosphere led to simultaneous

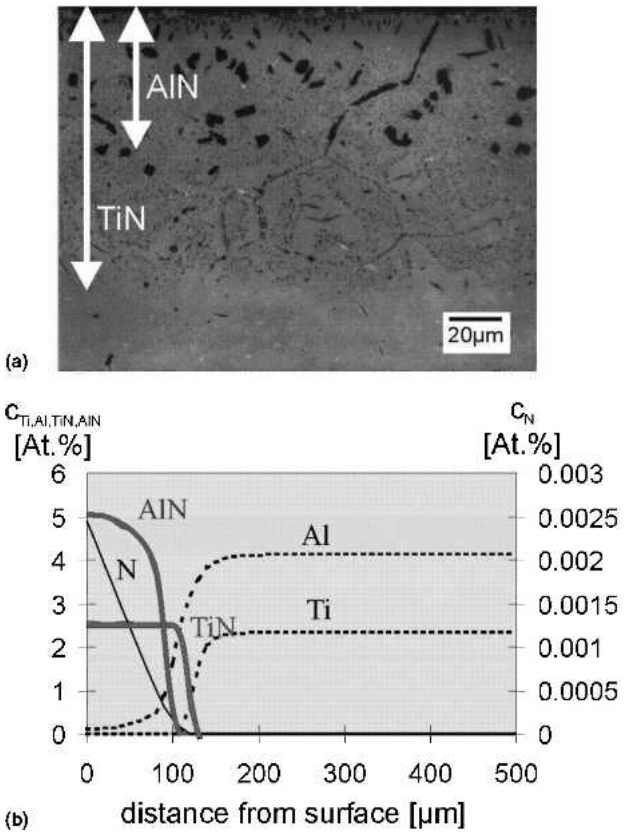

Fig. 9 Simultaneous internal precipitation of TiN and AlN in Ni-20wt.%Cr-2wt.%Al-2Ti alloy (100 h, 1000 °C, nitrogen-based atmosphere): (a) cross section; and (b) corresponding simulated concentration profiles[16]

internal nitridation of Al and Ti. Within the precipitation zone of TiN as the most stable nitride compound, less stable Al nitrides are formed decreasing the nitrogen flux to the TiN reaction front. Such a situation is not covered by the fundamental Eq 4 and 5 of internal oxidation, and hence, this kind of multiphase internal corrosion should be a representative example for the useful application of a numerical treatment. Figure 9(a) shows an SEM micrograph of a nitrided cross section of a Ni-20wt.%Cr-2wt.%Al-2wt.%Ti alloy in comparison with the concentration profiles of the species involved in the nitridation process calculated by the finite-difference model introduced in section 3 (Fig. 9b). Obviously, the rate of internal nitridation is again mainly determined by the diffusion of dissolved nitrogen within the zone of internal precipitation. The effect of the counterdiffusion of Al and Ti seems to be small, and hence, the well-known enhancement of the interdiffusion of Al in commercial Ni-base alloys containing Cr and Al seems to be not of significance with respect to the progress of the internal nitridation front.

The simulation results are in reasonable agreement with the measured nitride penetration depth (compare Fig. 9a). The overestimation of the AlN precipitation depth can be attributed to the simplifying assumption that the nucleation and growth kinetics of the precipitates are negligible.

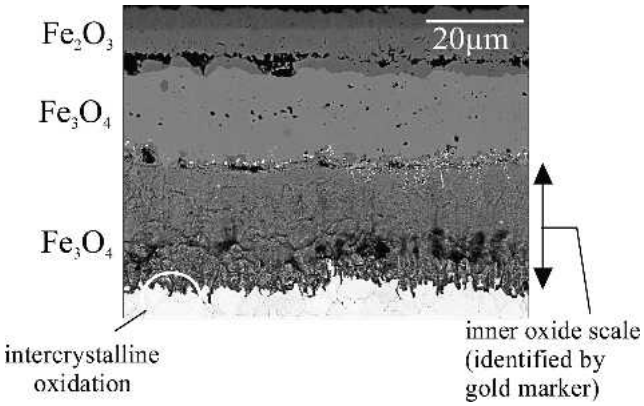

Fig. 10 Cross section of the low-alloy steel X60 (c_{Cr} = 1.44 wt.%) after 72 h of exposure to air at 550 °C[20]

The large and blocky morphology of the AlN precipitates compared with the TiN precipitates and the fact that the measured precipitation depth is lower than the calculated depth can be seen as some evidence that the interfacial energy is a vital factor to be taken into account to understand and to precisely predict internal corrosion kinetics.

5. Intercrystalline Oxidation of Boiler Steels

At very high temperatures in the range between approximately 900 and 1100 °C, the role of grain-boundary diffusion within internal corrosion processes can be neglected, as is shown in Fig. 9, and although the grain boundaries act as the preferred nucleation site, the depth of the internal TiN precipitation zone is uniform. However, in the moderate temperature regimen between approximately 500 and 900 °C, grain-boundary diffusion might be the rate-determining step for many high-temperature corrosion processes. Hence, the simulation of such processes requires the implementation of the microstructural parameters of the material.

The oxidation of Cr-containing steels, which are used, for example, as superheater tubes or waterwalls in power plants, is an example for corrosion processes that depend strongly on interfacial diffusion. By applying an inert gold marker on the surface of unexposed samples, it was shown that oxidation of low-alloy Cr steels ($c_{Cr} \approx$ 1...2.5 wt.%) at a moderate temperature of 550 °C is a combination of outward growth of hematite (Fe_2O_3, outermost) and magnetite (Fe_3O_4), and inward growth of magnetite, which gradually enriches in Cr forming the complete $FeCr_2O_4$ spinel phase at the scale-substrate interface. This is shown in Fig. 10 for the example of the tube steel X60.[20] Underneath the scale-substrate interface, preferential oxidation attack along the grain boundaries can be observed. Hence, it is proposed that inner scale growth is driven by an intercrystalline oxidation mechanism that requires oxygen transport via anion diffusion, pores, or cracks through the magnetite scale, establishing an oxygen concentration at the scale-substrate interface that corresponds to the Fe_3O_4 dissociation pressure. Initially, intercrystalline oxidation is assumed to be restricted to the formation of the most stable Cr_2O_3 and $FeCr_2O_4$, respectively, driven by the inward diffusion of oxygen along the substrate grain boundaries and the bulk.

In the computer model introduced in section 3, this process is described by a two-dimensional finite-difference area, where the elements of the location-dependent oxygen diffusion coefficient matrix are set to the grain-boundary diffusion coefficient D_{GB}, which is assumed to be larger by a factor of 100 than the bulk diffusivity of oxygen in Fe of[21]:

$$D_{\text{O in }\alpha\text{Fe}} = 2.8 \cdot 10^{-4} \frac{\text{m}^2}{\text{s}} \exp \frac{-251\text{kJ/mol}}{RT}\ [20] \qquad \text{(Eq 15)}$$

The oxygen transport from the outer-inner scale interface [$p(O_2)'$] to the scale-substrate interface [$p(O_2)''$] has been treated by an approximate effective diffusion coefficient $D_{O,eff}$ that was derived from the measured inner oxide-scale thickness data, by which the parabolic rate constant k_p was obtained, in combination with Wagner's theory of oxidation.[22]

$$k_p = \int_{p(O_2)'}^{p(O_2)''} D_{O,eff} \ln p(O_2) \qquad \text{(Eq 16)}$$

Using the diffusion coefficients for the grain-boundary and bulk transport of oxygen into the substrate and for effective oxygen transport through the inner oxide scale, as mentioned above in combination with a tailor-made database for high-temperature corrosion of boiler steels,[23] the concentration profiles of the oxidation products during the inward oxide scale growth can be predicted by means of the finite-difference approach introduced in section 3. Figure 11(a) shows as an example the calculated magnetite concentration in a two-dimensional area with one grain boundary. Once a row of elements of the grain interior is completely oxidized, it is treated as part of the inner oxide scale (i.e., the thickness of the oxide scale has been grown by an increment of width Δy).

Figure 11(b) shows the predicted inner-oxide thickness versus the experimental data, which are in excellent agreement. In addition to this, the two-dimensional finite-difference approach allows the simulation of corrosion processes in materials of various grain sizes. Hence, it is capable of describing the experimentally observed increase in the oxidation rate of low-Cr steels with decreasing grain size (higher fraction of grain boundaries as fast-diffusion paths; see Ref 20 and Fig. 11b).

6. Conclusions

Even though Wagner's classic theory of internal oxidation can be used to estimate the kinetics of many internal corrosion processes, its applicability is limited when (a) one or more compounds of moderate thermodynamic stability are involved, (b) the surface concentration of the corrosive species is not constant due to the growth and failure of an outer scale, or (c) if various diffusion paths (e.g., bulk and grain-boundary diffusion) have to be taken into account.

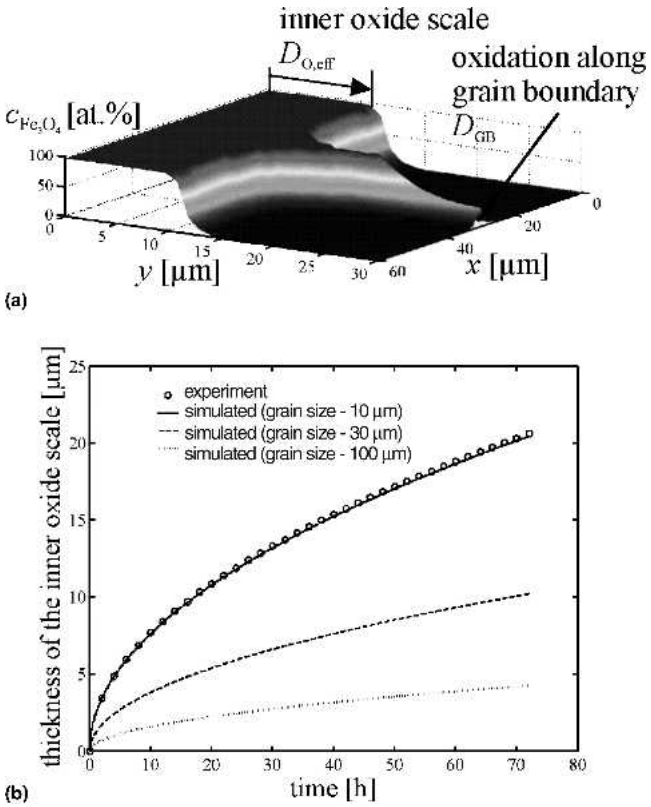

Fig. 11 (a) Simulated Fe_3O_4 concentration profile, and (b) comparison of experimentally determined and calculated inner-oxide scale thickness for exposure of the steel X60 to air at 550 °C[20]

These limitations can be overcome by a numerical approach combining the finite-difference technique for the treatment of diffusion processes with computational thermodynamics.

The two examples given in the present article for the application of such a numerical simulation model to internal nitridation of Ni-base alloys and intercrystalline oxidation of Cr steels are representative for many technical internal corrosion problems (e.g., internal carburization or internal sulfidation), which can be treated in a similar manner.

Acknowledgments

The financial support of Deutsche Forschungsgemeinschaft (DFG) and the European Commission is gratefully acknowledged. The authors would like to thank Dr. S.Y. Chang, R. Orosz, U. Buschmann, V. Braz Trindade, and Prof. W. Wiechert for their experimental contributions and fruitful discussions.

References

1. J.L. Meijering, Internal Oxidation in Alloys, *Advances in Materials Science,* H. Hermann, ed., Wiley, New York, 1971, p 1-81
2. P. Kofstad, *High Temperature Oxidation of Metals,* 1st ed., Electrochemical Society, London, 1966
3. H.W. Grünling and R. Bürgel, Influence of High-Temperature Corrosion on the Mechanical Properties at High Temperatures, *Werk. Korros.,* Vol 34, 1987, p 527-538 (in German)
4. V.P. Swaminathan and J.M. Allen, Surface Degradation and Cracking in Combustion Turbine Blade Cooling Passage, *Mater. Manufact. Proc*., Vol 10, 1995, p 867-885
5. R. Orosz, U. Krupp, and H.J. Christ, Study of the Oxide Scale Integrity on Ni-Base Alloy CMSX-4 During Isothermal and Thermal-Cycling Exposure, *Mater. Corros.,* 2005, in press
6. C. Wagner, Reaction Types During Oxidation of Alloys, *Z. Elektrochem.,* Vol 63, 1959, p 772-782 (in German)
7. R.A. Rapp, The Transition from Internal to External Oxidation and the Formation of Interruption Bands in Silver Indium Alloys, *Acta Metall.,* Vol 9, 1961, p 730-741
8. D.L. Douglass, A Critique of Internal Oxidation in Alloys During the Post-Wagner Era, *Oxid. Metall.,* Vol 44, 1995, p 81-111
9. S.W. Guan, H.C. Yi, and W.W. Smeltzer, Internal Oxidation of Ternary Alloys: Part II—Kinetics in the Presence of an External Scale, *Oxid. Metall.,* Vol 41, 1994, p 389-400
10. M. Udyavar and D.J. Young, Precipitate Morphologies and Growth Kinetics in the Internal Carburisation and Nitridation of Fe–Ni–Cr Alloys, *Corros. Sci,* Vol 42, 2000, p 861-883
11. F.H. Stott, Internal Oxidation, *Mater. Sci. Technol.,* Vol 4, 1988, p 1072-1083
12. G. Böhm and M. Kahlweit, On Internal Oxidation of Metallic Alloys, *Acta. Metall.,* Vol 12, 1964, p 641-648 (in German)
13. J. Crank, *The Mathematics of Diffusion,* 2nd ed., Clarendon Press, Oxford, 1986
14. G. Erickson and K. Hack, ChemSage: A Computer Program for the Calculation of Complex Chemical Equilibria, *Metall. Trans. B,* Vol 21, 1990, p 1013-1023
15. H.J. Christ, Experimental Characterization and Computer-Based Description of the Carburization Behaviour of the Austenitic Stainless Steel AISI 304L, *Mater. Corros.,* Vol 49, 1998, p 258-265
16. U. Krupp and H.J. Christ, Internal Nitridation of Nickel-Base Alloys: Part II—Behavior of Quaternary Ni-Cr-Al-Ti Alloys and Computer-Based Description, *Oxid. Metall.,* Vol 52, 1999, p 299-319
17. U. Krupp and H.J. Christ, Internal Nitridation of Nickel-Base Alloys: Part I—Behavior of Binary and Ternary Alloys of the Ni-Cr-Al-Ti System, *Oxid. Metall.,* Vol 52, 1999, p 277-298
18. U. Krupp, S.Y. Chang, and H.J. Christ, Precipitation of the Ternary π Phase during Nitriding of Ni-Cr and Ni-Cr-Ti Alloys and Thermodynamic Prediction Using the Ni-Cr-N System, *Z. Metallkd.,* Vol 12, 2000, p 1006-1012
19. H.J. Christ, S.Y. Chang, and U. Krupp, Thermodynamic Characteristics and Numerical Modelling of Internal Nitridation of Nickel Base Alloys, *Mater. Corros.,* Vol 54, 2003, p 887-894
20. V.B. Trindade, U. Krupp, Ph. Wagenhuber, and H.J. Christ, Oxidation Mechanisms of Cr-Containing Steels and Ni-Base Alloys at High-Temperatures: Part I—The Different Role of Alloy Grain Boundaries, *Mater. Corros.,* 2005, in press
21. I. Kaur, W. Gust, and L. Kozma, *Handbook of Grain and Interface Boundary Diffusion Data,* Ziegler Press, Stuttgart, Germany, 1989
22. C. Wagner, Contribution to the Theory of Scale Formation, *Z. Phys. Chem.,* Vol 21, 1933, p 25-41 (in German)
23. K. Hack, Development of Toolboxes for the Modelling of Hot Corrosion of Heat Exchanger Components, *Mater. Corros.,* 2005, in press